PERGAMON

International Journal of Solids and Structures 38 (2001) 8787–8803

INTERNATIONAL JOURNAL OF SOLIDS and STRUCTURES

www.elsevier.com/locate/ijsolstr

Modeling shock loading behavior of concrete

Danian Chen [a,*], S.T.S. Al-Hassani [b], Zhihua Yin [a], Yuying Yu [a]

[a] *Mechanics and Materials Science Research Center, Ningbo University, Zhejiang 315211, People's Republic of China*
[b] *Department of Mechanical Engineering, UMIST, Manchester, M60 1QD, UK*

Received 16 August 2000

Abstract

In order to tackle behavior of individual components in concrete cells under shock loading, a multi-part model for concrete is presented, wherein mortar and aggregate are assumed to be in mechanical equilibrium and compressed or released isentropically. Computational simulations of plate shock experiments using the multi-part model for concrete are performed. Computational velocity histories of the free surface of the target are compared with experimental results. Nonlocal response of the multi-part model for concrete to uniform shock loading is presented. The irregular aggregate distribution in actual concrete is replaced by a distribution of single-sized equally separate aggregates and the radius of influence surrounding each aggregate is given. The phenomena accompanied by the passage of a spherical shock wave through the mortar and aggregate are discussed. It is shown that Rayleigh–Taylor instability would cause separation of mortar and aggregate seriously for concrete with porous mortar at low initial density. It is shown that the behavior of the interface between mortar and aggregate under shock loading is captured qualitatively by the multi-part model for a simulated concrete cell. The multi-part model presented in this paper can be expected to numerically simulate shock loading behavior of concrete.

Keywords: Concrete; Shock wave; Multi-part model; Porous; Mesostructure

1. Introduction

Dynamic properties of concrete are not well understood. An empirical rate-dependent cap model (Chen et al., 2000) was proposed assuming that the effects of strain rate on the plastic loading surface and damage surface are separable and isolated from the static effect by considering the strength enhancement at high strain rates. Using the proposed rate-dependent constitutive model for concrete, the numerical simulations capture the overall qualitative behavior of concrete response to planar impact at different velocities. However, in order to be able to model the shock wave behavior, a nonlinear volumetric material behavior is required and shock equation of state properties of concrete has been developed by Grady (1996). Very little work was undertaken on the behavior of concrete under plate impact conditions because of the experimental difficulties involved. Concrete is a heterogeneous material and questions of hydrodynamic and

* Corresponding author. Tel.: +86-574-7604198; fax: +86-574-7600421.
E-mail address: chdnch@nbu.edu.cn (D. Chen).

0020-7683/01/$ - see front matter
PII: S0020-7683(01)00102-0

thermodynamic equilibrium behind the shock wave are very complicate. Since the shock wave not only sees components of different shock impedance but also travels through these components at different velocities. In this paper, a multi-part model for concrete under shock loading is presented, computational simulations of plate shock experiments using the multi-part model for concrete are performed and the nonlocal response of the multi-part model for concrete to uniform shock loading is discussed. It is shown that the multi-part model can be expected to numerically simulate shock loading behavior of concrete.

2. A multi-part model for concrete under shock loading

A unit cell for concrete presented in this paper consists of mortar and aggregate with known Hugoniots. It has been found (Shi et al., 1999) that Hugoniots of mortar and aggregate can be adequately represented by the linear relationship

$$U_s = C_0 + \lambda U_p \tag{2.1}$$

where U_s is the shock velocity, U_p the particle velocity, and C_0, λ the constants (in certain velocity region).

The theoretical analysis of the equation of state for mixtures is very complex and has not been carried out yet. There are several interpolation methods that could be used in an attempt to predict the equation of state for mixtures from the known Hugoniots of their components.

The method recommended by Mcqueen et al. (1970) is as follows:

- Construct the 0 K pressure–volume plot from the Hugoniot for each element.
- Mix the 0 K isotherm on a mass fraction basis and obtain the 0 K isotherm for the mixture.
- Obtain the equation of state for the mixture from the 0 K isotherm.

A much simpler method (Meyers, 1994) is based on the interpolation of the C_0 and λ values in Eq. (2.1) by mass averaging.

Thus, the equation of state for the unit cell consisting of mortar and aggregate can be predicted with varying degrees of rigorousness and the gross shock loading behavior of concrete can be simulated numerically using hydrocodes. However, the question remains of how to consider the shock loading behavior of individual components in the unit cell. It was noted (Bischoff and Perry, 1995) that little evidence was available to suggest crack propagation through the aggregate particles during impact loading despite suggestion to the contrary (Bischoff and Perry, 1991). Here, a multi-part model will be given to unit cells, wherein the two components are modeled with separate meaning. In reality, the failure process in concrete can be explained by the mesostructure of mortar and aggregate and the interaction between them.

We assume that the two components are in mechanical equilibrium,

$$P_m(V_m, E_m) - P_a(V_a, E_a) = 0 \tag{2.2}$$

where P is the pressure, V the specific volume, E the specific energy and subscripts m and a refer to mortar and aggregate, respectively. It is desired to sum the specific volume and energy since these are additive for the mixture.

$$E = m_a E_a + (1 - m_a) E_m \tag{2.3}$$

$$V = m_a V_a + (1 - m_a) V_m \tag{2.4}$$

where

$$m_a = M_a/(M_a + M_m) \tag{2.5}$$

where M is the mass.

In addition to Eqs. (2.2)–(2.4), we consider the isentropic compression and expansion of individual components in the unit cell in order to determine V_a, E_a, V_m and E_m from V, E for the unit cell. In fact, achievement of temperature equilibrium between different components of the mixture depends on grain size. If no heat flow occurs, individual components are compressed and released isentropically. It can be inferred from the conservation law of energy that

$$\dot{E}_a - V_a W_a + P_a \dot{V}_a = 0 \tag{2.6}$$

holds, where the dot means a time derivative along a particle path and W_a is equal to stress deviators times velocity strains. The proposed way to tackle behavior of individual components in unit cells is as follows:

- Obtain gross specific volume V and energy E of unit cells using a finite difference procedure for conservation equations of mass, momentum and energy.
- Determine individual specific volume (V_a, V_m) and energy (E_a, E_m) for aggregate and mortar in unit cells by solving Eqs. (2.2)–(2.4) and (2.6).
- Calculate equilibrium pressure p from the equation of state for mortar or aggregate and complete a cycle for the finite difference procedure.

Obviously, the multi-part model presented above is different from the usual multi-phase fluid flow community, in which the set of equations consists of the conservation laws of mass, momentum and energy for each phase.

3. Computational simulation of plate shock experiments using the multi-part model for concrete

For one-dimensional elastic–plastic flow, the principal equations for plane ($d = 1$), cylindrical ($d = 2$) and spherical ($d = 3$) geometries are:

$$\frac{\dot{V}}{V} = \frac{1}{r^{d-1}} \frac{\partial (r^{d-1} U)}{\partial r} \tag{3.1}$$

$$\frac{\dot{U}}{V} = \frac{\partial \sigma_r}{\partial r} + (d-1) \frac{\sigma_r - \sigma_\theta}{r} \tag{3.2}$$

$$\dot{E} - V[S_1 \dot{\varepsilon}_1 + (d-1) S_2 \dot{\varepsilon}_2] + (p+q)\dot{V} = 0 \tag{3.3}$$

where U is the velocity; r the coordinate; $\sigma_r = -(p+q) + S_1$; $\sigma_\theta = -(p+q) + S_2$; S_1, S_2 are stress deviators; and $\dot{\varepsilon}_1$, $\dot{\varepsilon}_2$ the strain rates, q is the artificial viscosity and given by (Wilkins, 1980)

$$q = C_3^2 (\Delta U)^2 / V + C_4 (PV)^{1/2} |\Delta U| / V \tag{3.4}$$

where $C_3 = 2.0$ and $C_4 = 0.8$.

As mentioned earlier, it has been found that the Hugoniots of mortar and aggregate can be adequately represented by Eq. (2.1). Therefore, the following form (Wilkins, 1973) of Gruneisen equation of state is adopted for mortar and aggregate, respectively:

$$P = k_1 \widetilde{X} + k_2 \widetilde{X}^2 + k_3 \widetilde{X}^3 + \tilde{\gamma}_0 E \tag{3.5}$$

where

$$\begin{aligned}
\widetilde{X} &= 1 - V/V_0 \\
k_1 &= C_0^2/V_0 \\
k_2 &= C_0^2(2\lambda - \tilde{\gamma}_0/2)/V_0 \\
k_3 &= C_0^2\lambda(3\lambda - \tilde{\gamma}_0)/V_0 \\
\tilde{\gamma}_0 &= \text{Gruneisen parameter.}
\end{aligned} \tag{3.6}$$

The cohesion and compaction behavior of concrete results in an increasing resistance to shear up to a limiting value of yield strength as the loading increases. This is modeled in the present literature by Mohr–Coulomb model. Note that although the yield stress is pressure dependent and expressed by Eq. (3.7), the flow rule is volume independent, i.e. of the Prandtl–Reuss type.

$$\begin{aligned}
Y/\sqrt{3} &= A_1 + A_2\exp(-3p/A_3) + A_4\exp(-3p/A_5) \\
A_5 &= J_{10}/n \\
A_4 &= -[A_1 + A_2\exp(J_{10}/A_3)]\exp(-n)
\end{aligned} \tag{3.7}$$

where Y is the yield stress and A_1, A_2, A_3, J_{10}, n are various parameters.

The finite difference equations for Eqs. (3.1)–(3.4) are available (Wilkins, 1973). Gross specific volume V and energy E of unit cells are obtained by using a finite difference scheme in which these equations are correct to second order of small quantities Δr and Δt, except for the terms containing q in Eq. (3.2) and p in Eq. (3.3), where the conservation equation of energy (3.3) is not coupled with the equation of state for unit cells. Solving Eqs. (2.2)–(2.4) and (2.6) with Newton–Raphson process and Gaussian elimination method, we determine individual specific volume (V_m, V_a) and energy (E_m, E_a) for mortar and aggregate in unit cells. Then we calculate the equilibrium pressure p from the equation of state for mortar or aggregate. The flow rule of Prandtl–Reuss type with yield stress given by Eq. (3.7) is adopted to calculate stress deviators and a cycle for the finite difference procedure is completed.

Very little work has been published on the shock loading behavior of concrete under plate impact conditions. Recently, unique shock compression experiments have been developed by (Grady, 1996). Two typical high-velocity impact examples are chosen to show the effectiveness of the present multi-part model for concrete under shock loading. The experimental parameters for the chosen tests are listed in Table 1.

The experimental and computational velocity histories of the free surface of the target are shown in Figs. 1 and 2 for examples 3.1 and 3.2, respectively. In Figs. 1 and 2, curves e are experimental data (Grady, 1996) and curves C are computational results using the present multi-part model with $m_a = 0.31$ and parameters listed in Table 2.

The parameters in Eq. (3.7) are as follows (Gupta and Seaman, 1979):

$$A_1 = 90.0\ \text{MPa}, \quad A_2 = -83.0\ \text{MPa}, \quad A_3 = 270.2\ \text{MPa}, \quad J_{10} = 61.0\ \text{MPa}, \quad n = 1.0.$$

Table 1
Impact experiment parameters

	Driver plate (concrete)		Target plate (copper) Thick (mm)	Impact velocity (km/s)	C_0 (km/s)	λ
	Density (g/cm^3)	Thick (mm)				
Example 3.1	2.3	25.4	2.39	2.15	3.1	1.5
Example 3.2	2.3	25.4	2.33	1.74	3.0	1.7

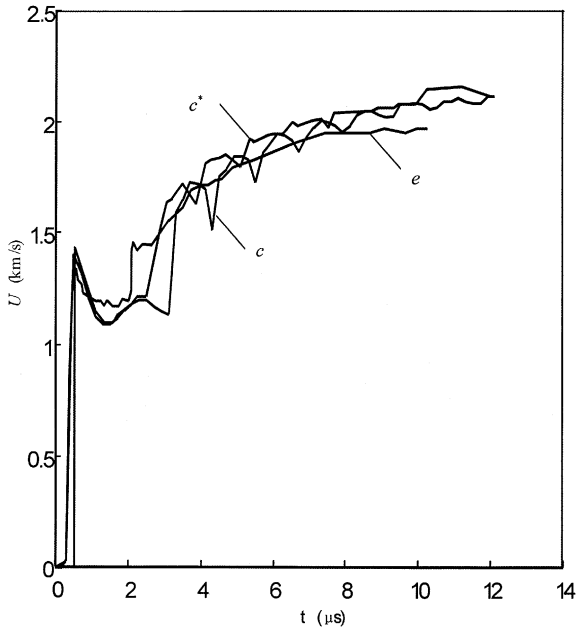

Fig. 1. The experimental and computational velocity histories of the free surface of the target for example 3.1.

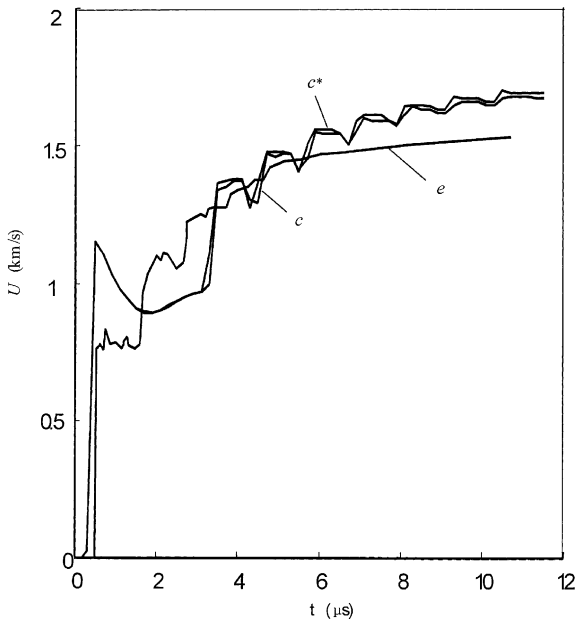

Fig. 2. The experimental and computational velocity histories of the free surface of the target for example 3.2.

Grady (1996) implied that a linear shock velocity versus particle velocity relation for concrete is existent and the parameters C_0 and λ for these examples are listed in Table 1. In Figs. 1 and 2, curves C^* are our computational results using Gruneisen equation of state with these parameters for concrete. In Figs. 3 and 4

Table 2
Parameters in Eq. (3.6) for examples 3.1 and 3.2

	V_0 (cm^3/g)	C_0 (km/s)	λ	$\tilde{\gamma}_0$
Mortar	0.46	2.3	0.81	0.62
Aggregate	0.38	2.43	1.52	2.05

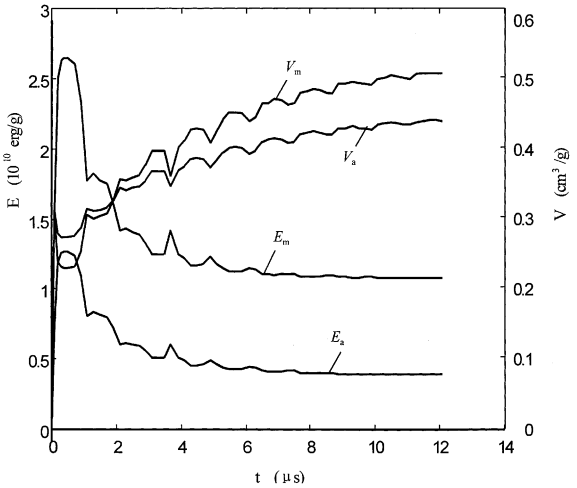

Fig. 3. The variations V_m, V_a, E_m and E_a in concrete near the concrete–copper interface with time for example 3.1.

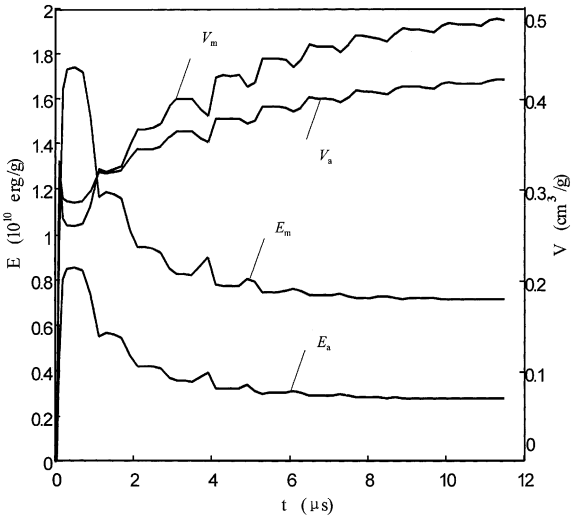

Fig. 4. The variations V_m, V_a, E_m and E_a in concrete near the concrete–copper interface with time for example 3.2.

the variations of V_m, V_a, E_m and E_a in concrete near the concrete–copper interface with time are given for examples 3.1 and 3.2, respectively.

4. Nonlocal response of the multi-part model for concrete to uniform shock loading

We will look in more detail, at the mesoscopic level, at what happens during the passage of the shock wave. The mesostructure of the multi-part model for concrete are related to the nonlocal response of concrete to shock loading. A simplified description of concrete can be obtained by repeating presented unit cells distributed uniformly throughout the material. The irregular aggregate distribution in actual concrete is to be replaced by a distribution of single-sized equally separated aggregates. The radius b of influence surrounding each aggregate is shown in Fig. 5 and can be estimated by

$$b = [(M_m V_m / M_a V_a) + 1]^{1/3} a \tag{4.1}$$

where a is mean radius of aggregate.

For a unit cell of concrete shown in Fig. 5, the phenomena accompanied by the passage of a spherical shock wave through the mortar and aggregate are of fundamental interest in the study of micromechanics of concrete under intense dynamic loading. When an impulsive pressure $p(t)$ is applied on the exterior surface of the unit cell, the shock front is formed. In the course of its propagation, the intensity and the velocity of the wave increase with increasing distance. If the shock has an intensity sufficient to vaporize the mortar or aggregate, the converging shock front moves according to the law $R = (-t)^{\tilde{\alpha}}$, the velocity U, density ρ and pressure P behind the front are:

$$\rho = \rho_0(\gamma + 1)/(\gamma - 1) \tag{4.2}$$

$$U = 2\dot{R}/(\gamma + 1) \sim R^{-(1-\tilde{\alpha})/\tilde{\alpha}} \tag{4.3}$$

$$P = 2\rho_0 \dot{R}^2/(\gamma + 1) \sim R^{-2(1-\tilde{\alpha})/\tilde{\alpha}} \tag{4.4}$$

where γ is polytropic coefficient.

$\tilde{\alpha} = \tilde{\alpha}(\gamma)$ can be expressed by the approximation of Whitham (1958). However, Eqs. (4.2)–(4.4) are only valid for a perfect gas. A general equation of state $E = E(P, V)$ involves dimensional parameters and the

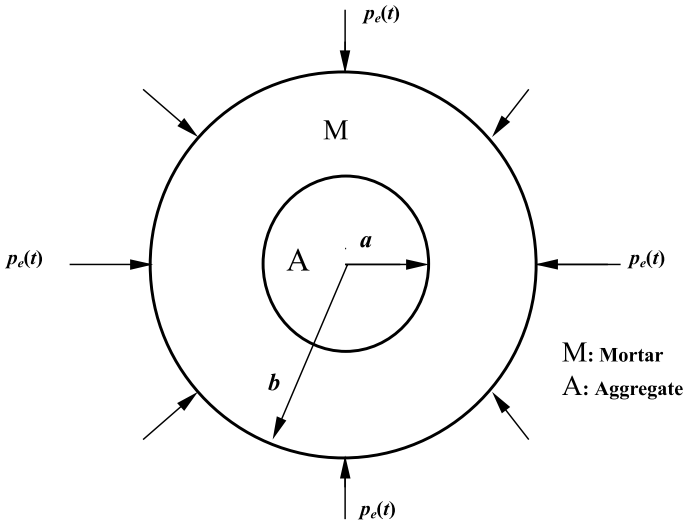

Fig. 5. A unit cell used in modeling the nonlocal response of concrete to uniform shock loading.

self-similar solution exists no more. Moreover, a converging shock could be unstable and cumulative processes cannot be perfect. Cumulation processes and self-similar solutions in gas dynamics have been reviewed by Somon (1971). As the intensity of the shock becomes just enough to liquefy the mortar or aggregate, the behavior of this liquefied zone is hydrodynamic. For a certain value of the wave's pressure peak, the mortar or aggregate is subjected to the passage of the wave to stresses greater than its dynamic crushing strength, it is crushed consequently. The fracture of a rock which is due to shock compression was discussed by Maury and Levret (1972). It is assumed that the fracture due to compression occurs when the strain energy per unit volume referring to the distortion reaches a certain value. When the mortar or aggregate is crushed by the shock, it may be roughly likened to sand. Under these conditions, the mechanical properties of the material are comparable with those of a soil. In addition, the failure mechanisms involving presented unit cells in compression under impact or explosive loading are supposed to be connected with the Rayleigh–Taylor instability. In the course of shock propagation, superposed mortar and aggregate are accelerated in a direction perpendicular to their interface and this interface is unstable according to Rayleigh–Taylor instability. Defining the amplification factor of an unstable fluid surface as the ratio of η the amplitude of the disturbance at any time to η_0 its initial value, Taylor found (Taylor, 1950) for acceleration $g1 \gg g$ (g acceleration of gravity)

$$\frac{\eta}{\eta_0} = \cosh \sqrt{\left\{4\pi\tilde{m}(\rho_2 - \rho_1)/(\rho_2 + \rho_1)\right\}} \tag{4.5}$$

where $\tilde{m}$ is the number of wavelengths that the liquid has descended. Thus, the amplification of an unstable disturbance depends only on the ratio of the densities of the two fluids and the number of wavelengths through which they have descended.

Obviously, the analytical study on the response of the unit cell for concrete to uniform shock loading is difficult and the numerical study of this problem is beneficial to discussing the micromechanisms of failure of concrete. The influence of density distribution, characteristic lengths, porosity and shock behavior of mortar and aggregate on response of concrete to shock loading. A numerical scheme for studying this two-layer inclusion is implemented using the principal equations (3.1)–(3.3) with $d = 3$.

We assume that the porosity of concrete is concentrated in mortar. The equation of state of mortar could be given by Herrmann's p–α model (Herrmann, 1969) or Carroll–Holt model (Carroll and Holt, 1972). However, our problems of interest involve shock compaction of the porous mortar, i.e. the region of interest lies on or near the Hugoniot. Using Rankine–Hugoniot relations and the Mie–Gruneisen equation, a reliable calculation procedure for the equation of state of porous material was developed by Meyers (1994). The Hugoniot of mortar taking account of porosity can be given by

$$P_{\mathrm{H}} = \frac{[2V - \tilde{\gamma}(V_0 - V)]C_0^2(V_0 - V)}{[2V - \tilde{\gamma}(V_{00} - V)][V_0 - \lambda(V_0 - V)]^2} \tag{4.6}$$

where the subscript H is used for parameters along Hugoniot. C_0, λ and $\tilde{\gamma}$ are parameters in the linear relationship between shock and particle velocities and Gruneisen parameter for solid mortar, respectively. V_0 and V_{00} are initial specific volume of solid and porous mortar. Furthermore, for porous mortar, the Mie–Gruneisen equation of state will be used.

$$P_{\mathrm{m}} - P_{\mathrm{H}} = (E_{\mathrm{m}} - E_{\mathrm{H}})\tilde{\gamma}_{\mathrm{m}}/V_{\mathrm{m}} \tag{4.7}$$

where subscript m refers to mortar again.

$$E_{\mathrm{H}} = P_{\mathrm{H}}(V_{00} - V_{\mathrm{m}})/2 \tag{4.8}$$

Three typical examples are chosen to show the influence of porosity and characteristic lengths on response of concrete to shock loading. Parameters in Fig. 5 and Eq. (3.6) for examples are provided in Table 3.

Table 3
Parameters in Fig. 5 and Eq. (3.6) for examples

	Mortar					Aggregate				
	b (mm)	V_0 (cm^3/g)	C_0 (km/s)	λ	$\tilde{\gamma}_0$	a (mm)	V_0 (cm^3/g)	C_0 (km/s)	λ	$\tilde{\gamma}_0$
Example 4.1	1.46	0.46	2.3	0.81	0.62	0.95	0.38	2.43	1.52	2.05
Example 4.2	1.46	0.76	2.3	0.81	0.62	0.95	0.38	2.43	1.52	2.05
Example 4.3	14.6	0.46	2.3	0.81	0.62	9.5	0.38	2.43	1.52	2.05

The external surface in Fig. 5 is subjected to the following pressure $p_e(t)$, that is generated by a detonating explosive.

$$p_e(t) = 20\exp(-2t)\ \text{(GPa)} \tag{4.9}$$

where t is time (μs).

Computational variations of U, P, V_m, V_a, E_m, and E_a at the interface between mortar and aggregate with time for examples 4.1 and 4.2 are given in Figs. 6–11, respectively. For example 4.2, the initial distention of the mortar is 1.66 and Eq. (4.6) was adopted in the numerical simulation. However, calculated Hugoniots for porous materials using Eq. (4.6) deviate from measured at lower pressures substantially. We neglected pressure increase in compact process.

Figs. 6–11 show that the response of the unit cell for concrete to uniform shock compression is seriously influenced by the initial distention 1.66 of mortar. The shock wave deposits a great deal of energy in the porous mortar and raises higher pressure, internal energy at the interface between mortar and aggregate.

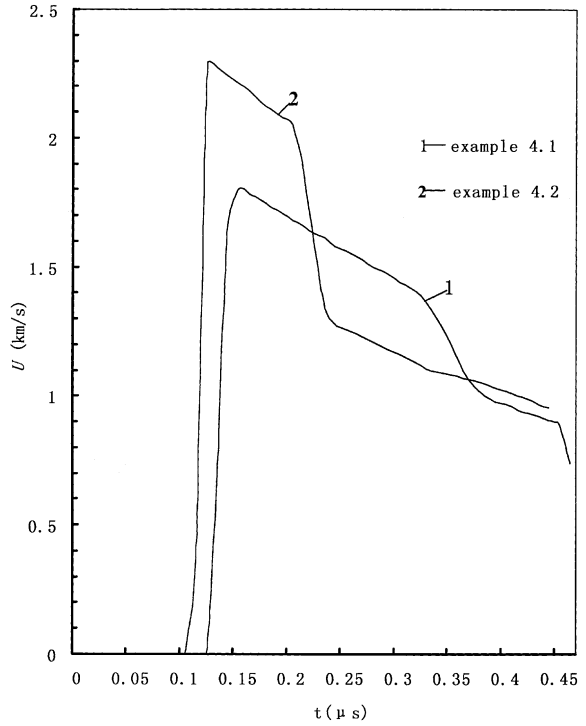

Fig. 6. Computational variations of velocity U at the interface between mortar and aggregate with time for examples 4.1 and 4.2.

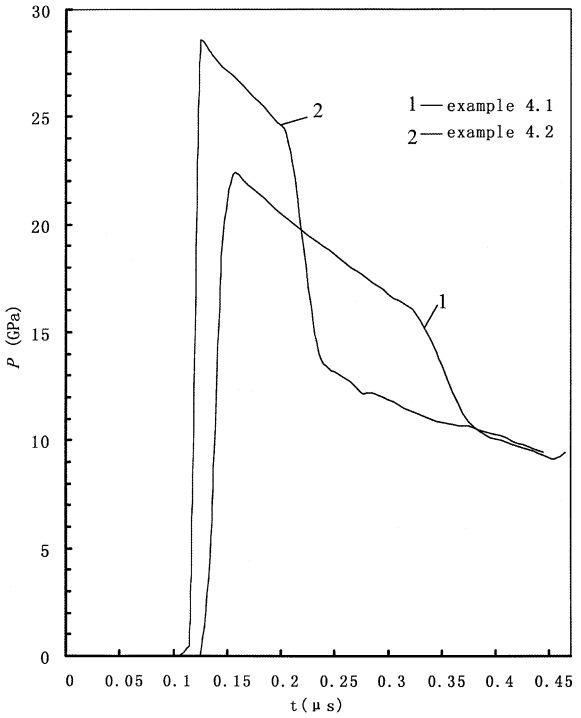

Fig. 7. Computational variations of pressure P at the interface between mortar and aggregate with time for examples 4.1 and 4.2.

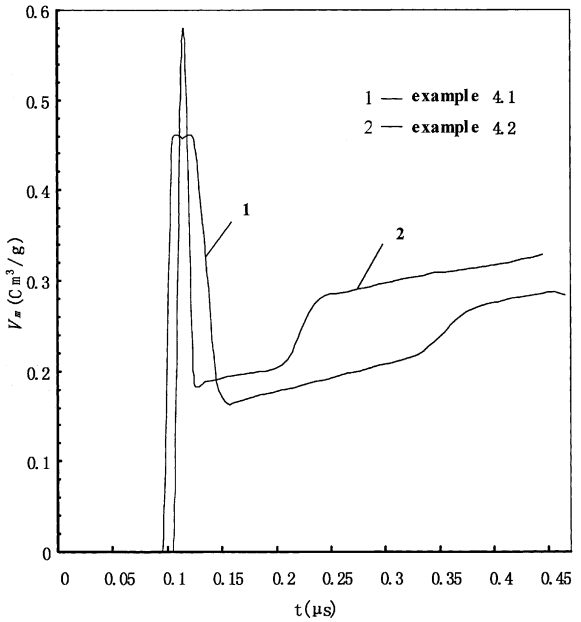

Fig. 8. Computational variations of specific volume V_m at the interface between mortar and aggregate with time for examples 4.1 and 4.2.

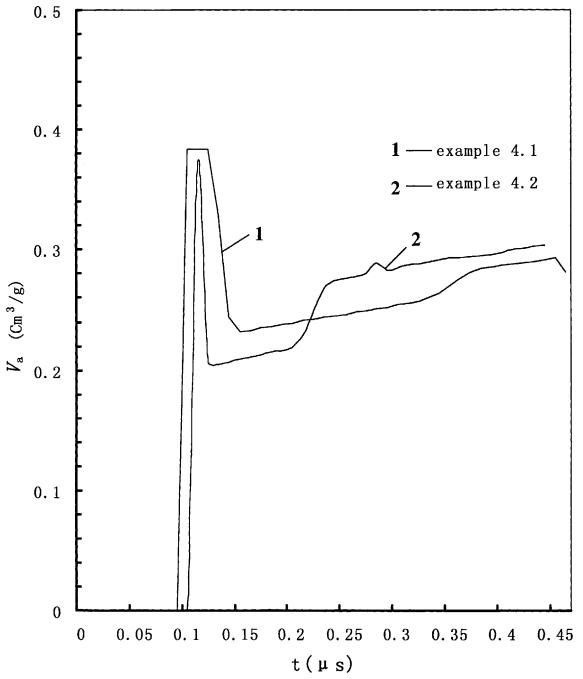

Fig. 9. Computational variations of specific volume V_a at the interface between mortar and aggregate with time for examples 4.1 and 4.2.

However, decay rates of these variables at the interface with time are higher in example 4.2 than in example 4.1. The fracture due to compression is assumed to occur when the strain energy reaches a certain value. Thus, it can be expected that the mortar and aggregate are both crushed more seriously or readily in example 4.2 than in example 4.1. In addition, it can be seen from Figs. 6, 8 and 9 that in the initial acceleration of the interface between mortar and aggregate under shock loading, the ratio of the densities of mortar and aggregate is greater in example 4.2 than in example 4.1. Therefore, the amplification factor of the unstable interface given by Eq. (4.5) is greater in example 4.2 than in example 4.1. Rayleigh–Taylor instability would cause separation of mortar and aggregate seriously for concrete with porous mortar at low initial density.

The concrete material contained 3/8 in. (9.5 mm) quartz aggregate is considered in example 4.3. Computational variations of U, P, V_m, V_a, E_m and E_a at the interface between mortar and aggregate with time for example 4.3 are given in Figs. 12–17.

Obviously, mesostructure lengths of concrete cells influence their response to shock loading. The continuum average stress has no meaning for concrete volumes smaller than that determined by the mesostructural heterogeneities of concrete. However, in general, the finite difference cell size for concrete could not be greater than the maximum aggregate size. For example 4.3, a simulated concrete cell with average density 2.3 g/cm^3 and spherical radius 14.6 mm is introduced and the multi-part model described in Section 2 is used to compute its response to the same loading. Computational variations of U, P, V_m, V_a, E_m and E_a at radius 9.5 mm are also shown in Figs. 12–17. It is shown from Figs. 12–17 that variations of velocity, pressure, specific volume and energy at the interface between mortar and aggregate with time for concrete contained 9.5 mm aggregate are captured qualitatively by the multi-part model for the simulated concrete cell. Therefore, the multi-part model presented in this paper can be expected to simulate shock loading behavior of concrete.

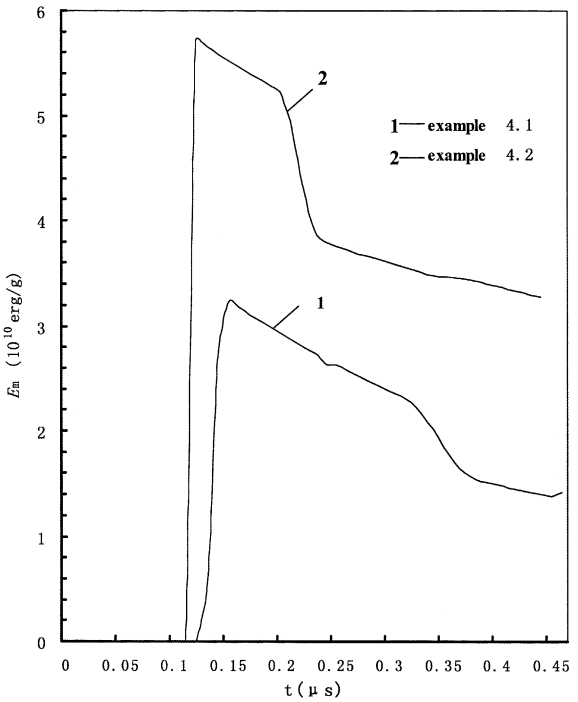

Fig. 10. Computational variations of specific energy E_m at the interface between mortar and aggregate with time for examples 4.1 and 4.2.

5. Conclusions

(1) In order to tackle behavior of individual components in concrete cells under shock loading, a multi-part model for concrete is presented, wherein mortar and aggregate are assumed to be in mechanical equilibrium and compressed or released isentropically, for achievement of temperature equilibrium between mortar and aggregate depends on grain size.

(2) Computational simulations of plate shock experiments using the multi-part model for concrete are performed. Computational velocity histories of the free surface of the target are compared with experimental results. Computational variations of specific volume and energy for mortar and aggregate in concrete near the fly plate–target plate interface with time are also given to show behavior of individual components in concrete under shock loading.

(3) Nonlocal response of the multi-part model for concrete to uniform shock loading is presented. The irregular aggregate distribution in actual concrete is replaced by a distribution of single-sized equally separated aggregates and the radius of influence surrounding each aggregate is given. The phenomena accompanied by the passage of a spherical shock wave through the mortar and aggregate are discussed.

(4) It is shown that the response of the unit cell for concrete to uniform shock compression is seriously influenced by the initial distention of mortar. Rayleigh–Taylor instability would cause separation of mortar and aggregate seriously for concrete with porous mortar at low initial density.

(5) It is shown that mesostructure lengths of concrete cells influence their response to shock loading. The behavior of the interface between mortar and aggregate under shock loading is captured qualitatively by the multi-part model for a simulated concrete cell. Thus, the multi-part model presented in this paper can be expected to numerically simulate shock loading behavior of concrete.

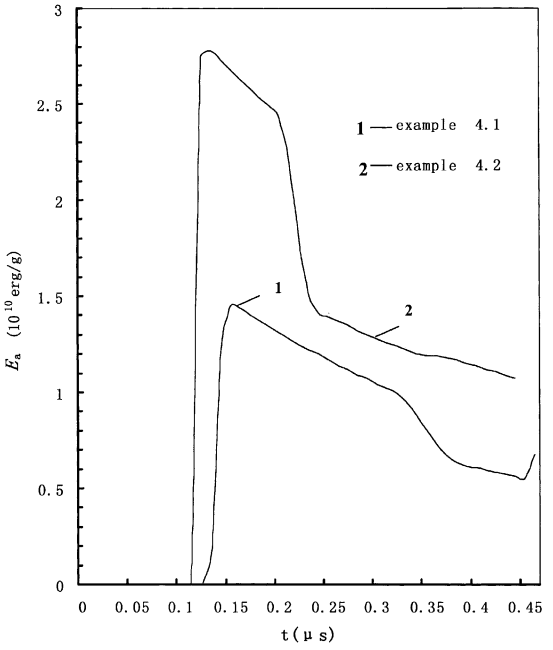

Fig. 11. Computational variations of specific energy E_a at the interface between mortar and aggregate with time for examples 4.1 and 4.2.

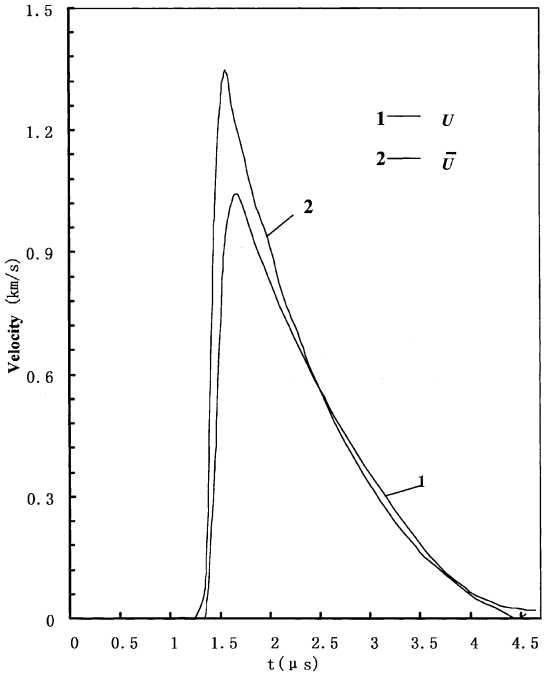

Fig. 12. Computational variations of velocity U at the interface between mortar and aggregate for example 4.3 and velocity $\overline{U}$ at radius 9.5 mm for a simulated concrete cell with time.

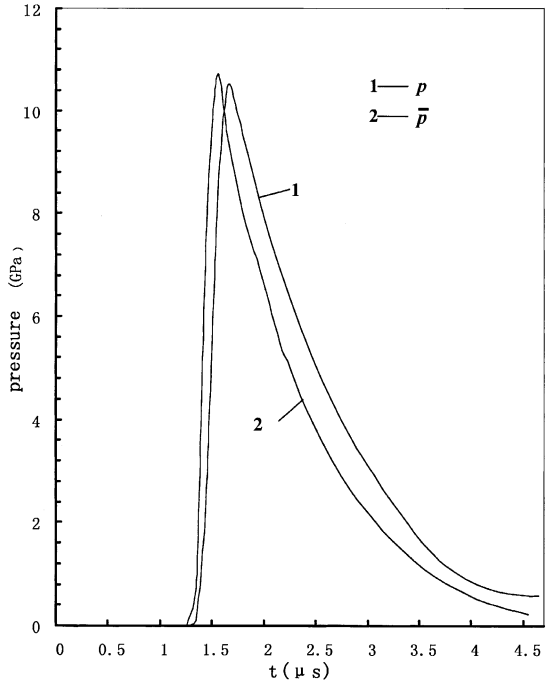

Fig. 13. Computational variations of pressure P at the interface between mortar and aggregate for example 4.3 and pressure $\bar{p}$ at radius 9.5 mm for a simulated concert cell with time.

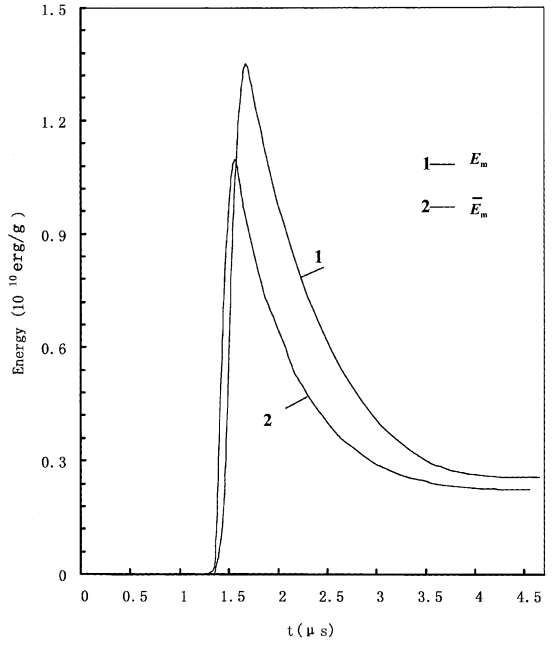

Fig. 14. Computational variations of specific energy E_{m} at the interface between mortar and aggregate for example 4.3 and specific energy $\overline{E}_{\mathrm{m}}$ at radius 9.5 mm for a simulated concrete cell with time.

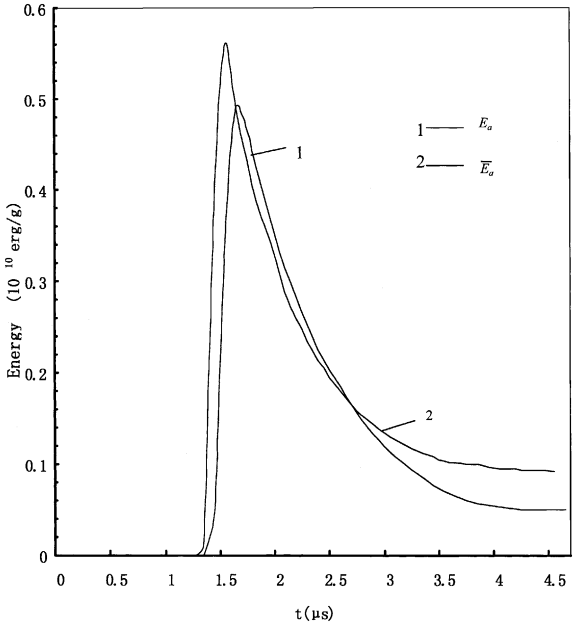

Fig. 15. Computational variations of specific energy E_a at the interface between mortar and aggregate for example 4.3 and specific energy $\overline{E}_a$ at radius 9.5 mm for a simulated concrete cell with time.

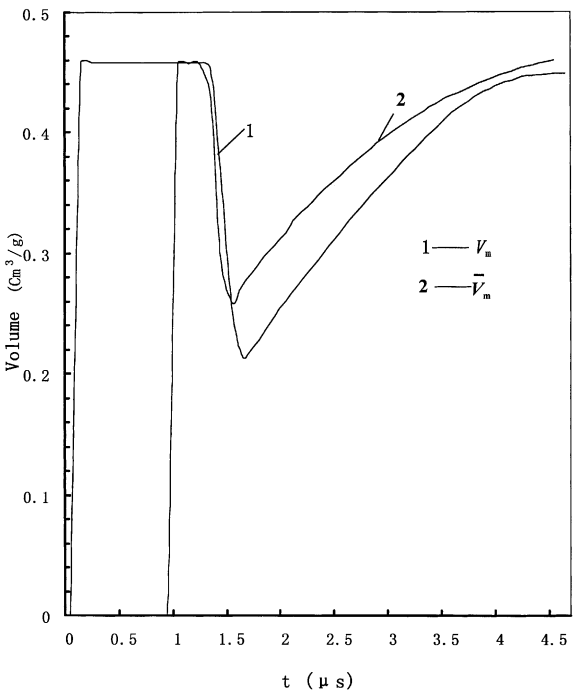

Fig. 16. Computational variations of specific volume V_m at the interface between mortar and aggregate for example 4.3 and specific volume $\overline{V}_m$ at radius 9.5 mm for a simulated concrete cell with time.

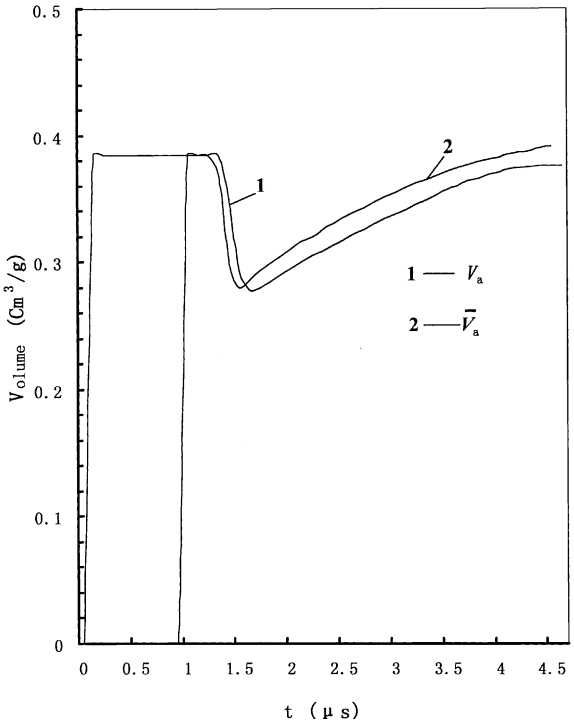

Fig. 17. Computational variations of specific volume V_a at the interface between mortar and aggregate for example 4.3 and specific volume $\overline{V}_a$ at radius 9.5 mm for a simulated concrete cell with time.

Acknowledgements

The authors wish to thank the National Natural Science Foundation of China and Science and Technology Funds of Laboratory for Shock Wave and Detonation Physics Research CAEP for their support.

References

Bischoff, P.H., Perry, S.H., 1991. Compressive behavior of concrete at high strain rates. Mat. Struct. 24, 425–450.

Bischoff, P.H., Perry, S.H., 1995. Impact behavior of plain concrete loaded in uniaxial compression. J. Engng. Mech. (June), 685–693.

Carroll, M.M., Holt, A.C., 1972. Static and dynamic pore collapse relations for ductile porous materials. J. Appl. Phys. 43, 1626.

Chen, D., Al-Hassani, S.T.S., Yin, Z., Gan, S., 2000. Rate-dependent constitutive law and nonlocal spallation model for concrete subjected to impact loading. Key Engineering Materials, vol. 177–180, Trans Tech Publications, Switzerland, pp. 261–266.

Grady, D., 1996. Shock equation of state properties of concrete. In: Jones, W., Brebbia, C.A., Watson A.J. (Eds.), Structures under Shock and Impact IV. Computational Mechanics Publications, pp. 405–414.

Gupta, Y.M., Seaman, L., 1979. Local response of reinforced concrete to missile impact. EPRI NP-1217, project 393-1, Final report, October.

Herrmann, W., 1969. Constitutive equation for the dynamic compaction of ductile porous materials. J. Appl. Phys. 40, 2490–2499.

Maury, J., Levret, C., 1972. Physics of phenomena in the close-in zone around underground nuclear explosions. UCRL-Trans-10617-8.

Mcqueen, R.G., Marsh, S.P., Taylor, J.W., Fritz, J.N., Carter, W.J., 1970. The equation of state of solids from shock wave studies. In: Kinslow, R. (Ed.), High-velocity Impact Phenomena. Academic Press, New York, pp. 294–415.

Meyers, M.A., 1994. Dynamic Behavior of Materials. Wiley–Interscience, New York, pp. 137–138, 140–146.

Shi, S., Chen, J., Li, D., Wang, L., 1999. Shock adiabatics of cement mortar at intense dynamical loading by taking into account the internal damage. Explos. Shock Waves (Special Issue) 19, 74–76.

Somon, J.P., 1971. Cumulation processes, Self-similar solutions in gas dynamics. In: Caldirola, P., Knoepfel, H. (Eds.), Physics of High Energy Density. Academic Press, New York, pp. 189–213.

Taylor, G., 1950. The instability of liquid surfaces when accelerated in a direction perpendicular to their planes. Proc. R. Soc. 201, 192–209.

Whitham, G.B., 1958. On the propagation of shock waves through regions of non-uniform area or flow. J. Fluid Mech. 4, 337–360.

Wilkins, M.L., 1973. Calculation of elastic–plastic flow. Lawrence Laboratory Report UCRL-7322.

Wilkins, M.L., 1980. Use of artificial viscosity in multidimensional fluid dynamic calculations. J. Comput. Phys. 36, 281–303.